

Fingerprints of intrinsic phase separation: magnetically doped two-dimensional electron gas

H. Terletska and V. Dobrosavljević

Department of Physics and National High Magnetic Field Laboratory, Florida State University, Tallahassee, FL 32310

In addition to Anderson and Mott localization, intrinsic phase separation has long been advocated as the third fundamental mechanism controlling the doping-driven metal-insulator transitions. In electronic system, where charge neutrality precludes global phase separation, it may lead to various inhomogeneous states and dramatically affect transport. Here we theoretically predict the precise experimental signatures of such phase-separation-driven metal-insulator transitions. We show that anomalous transport is expected in an intermediate regime around the transition, displaying very strong temperature and magnetic field dependence, but very weak density dependence. Our predictions find striking agreement with recent experiments on *Mn*-doped *CdTe* quantum wells, a system where we identify the microscopic origin for intrinsic phase separation.

Two basic routes to the metal-insulator transition have long been known: the Anderson [1] (disorder-driven) and the Mott [2] (interaction-driven) mechanism for electron localization. In many novel materials, however, the intermediate “bad metal” regime is reached by lightly doping a parent insulator. Here, a new possibility emerges - the tendency of the few available charge carriers to “condense” into a Fermi liquid - leading to phase separation [3]. However, charge neutrality precludes global phase separation, and the ground state becomes inhomogeneous [4] - even in the absence of impurities or disorder. Such inhomogeneities can assume various patterns [5], including bubbles, stripes, or checkerboard states, and may also cause glassy behavior even in the limit of very weak disorder [6, 7]. The relevance of nano-scale phase separation, in its many proposed forms, has been advocated for the bad metal regimes of cuprates [3, 4] and manganites [8], and even low density two-dimensional electron gases (2DEG) [9]. Still, in most of these cases, no clear and conclusive evidence has been presented that intrinsic phase separation (IPS) - as driving force for the metal-insulator crossover - dominates the bad metal regime. While good evidence exists that here the carrier concentration is indeed inhomogeneous, this could very well be caused by impurity effects.

To make progress in understanding the relevance of IPS, it would be very useful and important to identify a model system, that would satisfy the following criteria: (1) the microscopic origin for the tendency of phase separation can be established; (2) the system is clean enough to avoid extrinsic impurity effects; and (3) transport signatures can be identified that make it possible to distinguish IPS from spurious disorder effects. In this letter we concentrate on a specific physical system - magnetically doped 2DEG - where all these criteria can be satisfied. We formulate a simple theoretical model that describes IPS in this system, and present theoretical results predicting its transport properties in the metal-insulator crossover regime.

Magnetically doped 2DEG: ideal IPS model system. The criteria for observing IPS are not easy to satisfy in most available systems. In many cases, such as for the

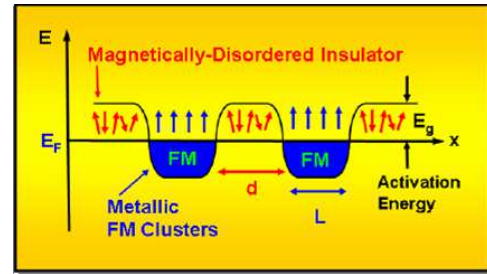


Figure 1: (Color online) In presence of magnetically-driven IPS, low-density carriers are trapped in ferromagnetic “bubbles” from which they can escape only by thermal activation. Such activation-limited transport results in resistivity which is a strong function of temperature and magnetic field, but a very weak density dependence - the smoking gun for IPS.

important family of doped cuprates [4], its microscopic origin remains highly controversial. In addition, chemical doping is typically linked with appreciable amount of disorder created by dopant ions; such is the situation in most manganite oxides and diluted magnetic semiconductors (DMS). Very recent experimental work [10], however, has presented striking results on a model system, which seems to be an ideal setting for observing IPS. Here, a standard 2DEG (formed in *CdTe* quantum wells) has been doped by Manganese - a situation that can be described as a two-dimensional DMS system. Because this 2DEG is created by (iodine) *modulation-doping*, the impurity ions are far from the mobile electrons, which dramatically reduces the disorder effects as compared to the well-known *CdMnTe* bulk (three dimensional) materials. As a result, the metallic behavior here persists down to remarkably low carrier densities, even under significant *Mn* doping. In addition, in this materials (as opposed to the more familiar *GaMnAs*), *Mn* is neither a donor nor an acceptor.

In this way, devices have been fabricated where, around the critical carrier density n_c , there are only a few percents of carriers per *Mn* ion. The possibility of reaching this regime is very significant, because it is precisely where one expects the *Mn*-induced magnetism to favor phase separation [8]. Indeed, both experimental and the-

oretical considerations have established [10] that $CdMnTe$ is, under sufficient carrier doping, a typical Zener (double-exchange) ferromagnet [11, 12]. In such materials sufficient doping induces ferromagnetic (FM) correlations between the Mn spins, which can prevail over the usual $Mn-Mn$ antiferromagnetic (AFM) superexchange that exists even in absence of carriers. At very low doping levels, however, the situation is more subtle. Here the *average* kinetic energy gain obtained by FM ordering is not sufficient to balance the energy cost of AFM superexchange that opposes it. Global FM is then not possible, but a compromise is reached through phase separation. FM ordering then prevails only in carrier-rich regions, where phase separation makes it possible to *locally* achieve a sufficient carrier concentration favoring Zener ferromagnetism.

Model. While the 2D $CdMnTe$ system offers an especially attractive venue to experimentally observe it, magnetically-induced IPS in a clean low density electron gas is a very robust phenomenon [8], not confined to two-dimensional systems or the specific material properties of $CdMnTe$. To emphasize its universal properties we concentrate on the simplest model that illustrates qualitative aspects of such an IPS, and is given by the Hamiltonian

$$H = H_{mag} + H_{Coul} + H_{imp}. \quad (1)$$

The first term here describes a (random) lattice of classical spins \vec{S}_i (representing the Manganese local moments), interacting with conduction electrons through “s-d” exchange interactions J_{sd} , and with each other through (AFM) superexchange interactions J_{ex} . Following Anderson and Hasegawa [12], for simplicity we focus on the $J_{sd} \rightarrow \infty$ limit, where the conduction electron spins completely align with the local moments

$$H_{mag} = - \sum_{ij} t \cos(\theta_{ij}/2) (c_i^\dagger c_j + c_j^\dagger c_i) + J_{ex} \sum_{\langle ij \rangle} \vec{S}_i \vec{S}_j. \quad (2)$$

Here, $\theta_{ij} = \arccos(\vec{S}_i \vec{S}_j)$ represents the relative angle between the neighboring Manganese spins, and c_i^\dagger is the conduction electron creation operator corresponding to lattice site i . The second term H_{Coul} represents the long-range Coulomb repulsion between conduction electrons; its principal role is to prevent global phase separation in order to keep the charge neutrality of the system. The last term H_{imp} describes (weak) disorder scattering, which in our system takes the form very similar as in other 2DEG materials not containing manganese spins.

IPS at $T=0$. To reveal the physical mechanism for IPS in our model, and understand the respective roles of the two magnetic interactions, we start our analysis by first constructing the ground state phase diagram for H_{mag} . In absence of superexchange ($J_{ex} = 0$), the ground state for any doping corresponds [12] to complete ferromagnetic (FM) polarization of all Mn spins, as this allows for maximum kinetic energy of conduction electrons. For $J_{ex} > 0$, however, at infinitesimal carrier

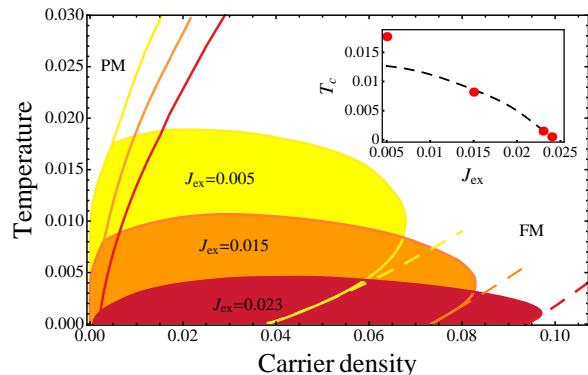


Figure 2: (Color online) DMFT phase diagram. Shaded areas show the IPS regions at three different values of J_{ex} . As J_{ex} increases, the critical density n_c increases, while the critical-end-point temperature T_c decreases, until IPS is suppressed at $J > J_{ex}^c \approx 0.025D$; the inset shows the analytical (dashed line) low-temperature approximation (see text) for $T_c(J_{ex})$, as compared to the numerical solution (dots). Note the “Pomeranchuk effect” - the re-entrance of the coexistence region, due to higher spin entropy of the carrier-poor PM phase.

doping the corresponding energy gain is not sufficient to overcome the cost of superexchange energy opposing spin alignment. No ferromagnetism is then possible, instead, the system undergoes phase separation between a FM carrier-rich phase, and a paramagnetic (PM) [17] carrier-poor (carrier-free at $T = 0$) phase. For our classical-spin model, the condition for IPS (phase coexistence) is obtained by equating the (grand) thermodynamic potentials of the respective phases, viz $\Omega_{FM} = \Omega_{PM}$. In the FM phase

$$\Omega_{FM} = \int_{-D}^{\mu} \rho(w) w dw + J_{ex}/2 - \mu \int_{-D}^{\mu} \rho(w) dw, \quad (3)$$

where $\rho(w)$ is the density of states of (spin polarized) conduction electrons, and $D \sim t$ is the corresponding half-bandwidth, while $\Omega_{PM} = 0$ [18]. We find that IPS emerges when the carrier density n (per Mn ion) satisfies the condition $n < n_c$, with

$$n_c \sim J_{ex}^{d/(d+2)}, \quad (4)$$

and $\mu_c + D \sim J_{ex}^{d/(d+2)}$. In the entire IPS regime, both the local carrier concentration in the FM phase $n_{FM} = n_c$, and the corresponding chemical potential $\mu_{FM} = \mu_c$ remain pinned at their critical value (independent of the average density n). As a result, the activation energy gap to the (PM) conduction band [19] $E_g = E_c - \mu$ also remains n -independent. This simple mechanism, common to any example of IPS, is the essential cause for very weak density dependence of (activated) transport in this regime.

Finite temperature phase diagram - DMFT solution. At finite temperatures, the situation is more complicated. First, a fraction of electrons are transferred from a carrier-rich FM domains into the carrier-poor PM regions. Second, at finite temperatures the entropy of spin

fluctuations strongly favors the PM phase. To quantitatively account for both of these effects, we now construct a complete phase diagram for our system using dynamical mean-field theory (DMFT). This approach, which is formally exact in the limit of large coordination, has recently been shown [8] to provide quantitatively accurate results even in low dimensions, for the class of models we consider. To determine the domain of magnetically-driven IPS, we first focus on effects described by H_{mag} ; we will later return to the role of H_{Coul} and its consequences on transport.

Within DMFT, the lattice model is reduced to solving a single-site quantum impurity model supplemented by an appropriate self-consistency condition. For our Anderson-Hasegawa model, the local effective action takes the form

$$S_{eff}(i, \vec{S}_i) = \int_0^\beta d\tau \int_0^\beta d\tau' c_i^\dagger(\tau) [\delta(\tau - \tau') (\partial_\tau + \mu) + \Delta_i(\tau, \tau', \vec{S})] c_i(\tau') - \beta J_{ex} m \vec{S}_i, \quad (5)$$

Here, we have used functional integration over Grassmann fields $c_i(\tau)$ describing electron at site i . The form of the self-consistency condition defining the ‘‘cavity field’’ $\Delta_i(\tau, \tau', \vec{S})$ depends on the electronic dispersion [13]. Within the DMFT, however, the results do not qualitatively depend on the precise form of the band structure or the dimensionality; without loss of generality we therefore use a simple semi-circular model bare density of states $\rho_0(\omega) = \frac{1}{D} \sqrt{D^2 - \omega^2}$. Using standard methods [13], we find

$$\Delta_i(w_n, \vec{S}) = (t^2/2)(G_{av}^{(i)}(w_n) + \vec{G}_m^{(i)}(w) \cdot \vec{S}), \quad (6)$$

where $G_{av}^{(i)}(w_n) = \langle c^\dagger(w_n)c(w_n) \rangle_{S_{eff}}$ and $\vec{G}_m^{(i)}(w) = \langle \vec{S}^\dagger(w_n)c(w_m) \rangle_{S_{eff}}$ are the local Green’s functions, and $m = \langle \vec{S} \rangle_{S_{eff}}$ is the magnetization. For simplicity, we also use Ising ($S = \pm 1$), as opposed to Heisenberg spins; we checked that within DMFT this only leads to very small quantitative changes. These DMFT equations are easy to solve numerically as a function of the carrier density and temperature, for several values of the superexchange J_{ex} ; the resulting phase diagram is presented in Fig. 2.

Temperature-driven IPS - Pomeranchuk effect. Our numerical solution reproduces Eq. 3 at $T = 0$, but interesting re-entrance (Fig. 2) is found at $T > 0$. Physically, the temperature increase favors phase separation, because of the larger spin entropy $S_{spin} \sim k_B \ln 2$ associated with the carrier-poor PM phase, very similar to the effect Pomeranchuk predicted for He^3 solidification. Very similar Pomeranchuk-like behavior of phase separation has been discussed for other systems [9], and generally it may give rise to pronounced resistivity maxima just on the metallic side of the MIT. To clarify this re-entrance, we note that the leading low-temperature behavior can be analytically obtained from Eqs. (5,6), by performing an appropriate Sommerfeld expansion. To

leading order $\Omega_{fm}(T) = \Omega_{fm}(T = 0) + O(T^2)$, while $\Omega_{pm}(T) = -k_B T \ln 2 + O(T^2)$, giving an expression for the high-density boundary of the coexistence dome (dashed line on Fig. 2) of the form

$$T_{coex}^+ = \frac{J_{ex}}{2k_B \ln 2} \left((n/n_c)^{(d+2)/d} - 1 \right). \quad (7)$$

A similar argument gives an expression for critical temperature of IPS

$$T_c(J_{ex}) \approx C(J_{ex}^c - J_{ex}), \quad (8)$$

where for our model $J_{ex}^c \approx 0.025D$, and $C \approx 0.88$. This shows, in perfect agreement with our numerics (see inset of Fig. 2), that while n_c increases with J_{ex} (see Eq. 4), the critical temperature T_c decreases, until phase separation is suppressed for $J_{ex} > J_{ex}^c$.

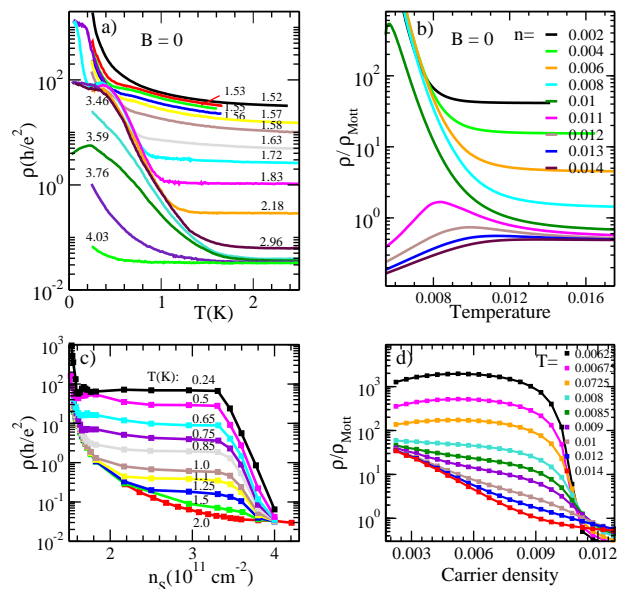


Figure 3: (Color online) (a) and (b) show the resistivity as function of temperature at different carrier densities. For comparison, we contrast the experimental results [10] (left panel) and our DMFT predictions (right panel). A sharp upturn in resistivity in the low temperature regime, and its weak density dependence are direct consequences of IPS. Plots (c) and (d) show the same data as function of carrier density at fixed temperatures to emphasize weak density dependence of resistivity below the percolation threshold. It also reflects the fact that within this region activation energy as well as the size of the PS regions is density independent (see text).

Phase separation and transport. As density increases in the IPS region, the volume fraction x of the carrier-rich FM phase determined from $n = xn_{FM} + (1-x)n_{PM}$ also increases, until a percolation concentration is reached and metallic transport sets in. In presence of long-range Coulomb interactions, the characteristic size of FM carrier-rich domains is limited by the charging energy, which can be easily estimated.

However, within a commonly-used random-resistor picture of transport (which is well known to be adequate for

the kind of system we consider) the critical behavior is largely insensitive to the individual domain size - with the only relevant parameter being the relative volume fraction x . Thus, to obtain a quantitative estimate of transport properties for our model, it suffices to calculate the local temperature-dependent resistivity for each of the two phases $\rho_{FM/PM}(n, T)$. This task is easily carried out using standard methods [13, 14] within DMFT model allowing us to determine the resistivity from the solution of our DMFT equations. This calculation accounts for density and temperature dependent resistivity $\rho_{FM/PM}(n, T)$ due to scattering of conduction electrons off Manganese spins in the respective phases.

To make a meaningful comparison with experiments, however, we also have to account for conventional impurity scattering while considering the total resistivity behavior. This weak impurity scattering in our system which, by the way, is unrelated to the physics of IPS and is more pronounced at higher temperatures, is of the same form as in conventional 2DEG systems [15]. In particular, as can be seen from the high-temperature transport data of Ref. [10], it has very weak temperature dependence but an appreciable density dependence, which we obtain by fitting the experimental data, giving $\rho_{imp} \approx \rho_o \exp\{-An\} + C$, (here we used $\rho_o = 3600\rho_{Mott}$, $A = 850$ and $C = 0.2\rho_{Mott}$; resistivity is in units of ρ_{Mott} [20]).

The net resistivity within the IPS region is then calculated by solving the random resistor problem, where we use the familiar effective-medium approximation (with ρ_{med} being determined as in (Eq. 5.7) of [16]), giving

$$\rho(n, T) = \rho_{med}(\rho_{fm}, \rho_{pm}) + \rho_{imp}.$$

The resulting resistivity curves are given in Fig. 3; as we can see, our model seems to capture all the qualitative features of the experimental data. Below the (temperature-dependent) percolation threshold, where we see a sharp increase in resistivity, the transport is activated with essentially density-independent activation energy. At higher densities, we note the well-pronounced resistivity maximum at low temperatures, reflecting the re-entrant Pomeranchuk-like IPS behavior we described above.

CMR behavior. As in other double-exchange ferromagnets, a moderate magnetic field reduces the IPS region, quickly lowers the relevant activation energy, and leads to colossal magnet-resistance (CMR) behavior (Fig. 4).

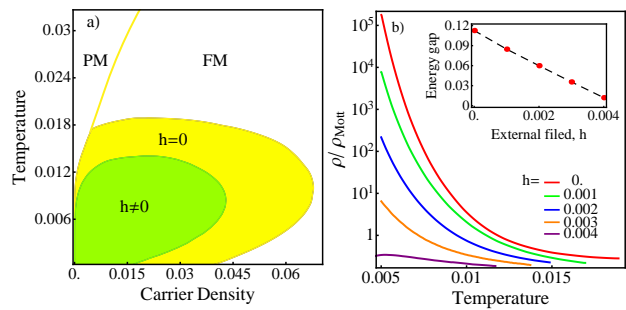


Figure 4: (Color online) Phase diagram (a) and transport (b) in presence of an external magnetic field h . Panel (a) shows how the temperature and density parameter range of IPS is quickly reduced in nonzero magnetic field, and (b) depicts the negative magnetoresistance within this IPS region (also seen in [10]). The inset of (b) shows the decrease of activation energy E_g (which was extrapolated from the resistivity vs. temperature plots) with magnetic field.

However, this behavior is restricted to the coexistence region, and as such can serve as an indication for IPS behavior-again in close agreement with experiments[10].

Conclusions. In this letter we presented and solved a simple microscopic model for magnetically-driven IPS behavior. Given the simplicity of our theoretical model, the agreement with all the qualitative features of the experimental data is remarkable. Most importantly, we observe how, within the IPS regime, all the resistivity curves “merge” together below a temperature scale set by T_c for phase separation. This striking feature simply reflects the fact that the chemical potential - setting the activation scale in this problem - is fixed and density-independent everywhere under the IPS dome. Such behavior is quantitatively reproduced in our model for magnetically driven IPS. However, very general thermodynamic principles guarantee that the very same behavior must be at play in virtually any system where transport is driven by a tendency to inherent phase separation - and not the disorder effects. In this work we identified the first physical system which presents plausible and convincing evidence for the IPS scenario. From a more general point of view, our results indicate how should one search for other examples where this fascinating physics may be recognized and properly interpreted.

We thank P. Schlottmann and S. von Molnar for fruitful discussion. This work was supported by the NSF grant DMR-0542026 and the National High Magnetic Field Laboratory.

[1] P. W. Anderson, *Phys. Rev.* **109**, 1492 (1958).
 [2] N. F. Mott, *Metal-Insulator Transition*. (Taylor & Francis, London, 1990).
 [3] L. P. Gor'kov *et al.*, *JETP Lett.* **46**, 420 (1987).
 [4] S. A. Kivelson *et al.*, *Rev. Mod. Phys.* **75**, 1201 (2003).
 [5] E. Dagotto, *Science* **309**, 257 (2005).
 [6] J. Schmalian *et al.*, *Phys. Rev. Lett.* **85**, 836 (2000).

[7] C. Panagopoulos *et al.*, *Phys. Rev. B*, **72**, 014536 (2005).
 [8] E. Dagotto, *Nanoscale Phase Separation and Colossal Magnetoresistance* (Springer-Verlag, Berlin, 2002).
 [9] R. Jaime *et al.*, *Phys. Rev. Lett.* **94**, 056805 (2005).
 [10] J. Jaroszyński *et al.*, *Phys. Rev. B*, **76**, 045322 (2007).
 [11] C. Zener, *Phys. Rev.* **82**, 403 (1951).
 [12] P. W. Anderson *et al.*, *Phys. Rev.* **100**, 675 (1955).

- [13] A. Georges *et al.*, Rev. Mod. Phys. **68**, 13 (1996).
- [14] B. M. Letfulov *et al.*, Phys. Rev. B, **64**, 174409 (2001).
- [15] T. Ando *et al.*, Rev. Mod. Phys., **54**, 437 (1982).
- [16] D. Belitz *et al.*, Rev. Mod. Phys. **66**, 261 (1994).
- [17] A more detailed analysis shows that our main conclusions are not significantly modified if one considers AF or spin glass ordering instead of PM solution we focus on.
- [18] We ignored any spin correlations in the PM phase
- [19] Due to random-spin orientation, the bandwidth is narrower in the PM phase; the corresponding band edge $E_c \approx -aD$, where $a \approx \langle \cos(\theta_{ij}) \rangle \approx 0.71$.
- [20] ρ_{Mott} is the Mott limit of the maximum metallic resistivity; to determine it we used $E_F\tau = 1$ (E_F is Fermi energy and τ is scattering time); N. E. Hossein *et al.*, Philosophical Magazine **84**, 2847 (2004).